Sorption of Europium on Diatom Biosilica as Model of a “Green” Sorbent for f-Elements

Kammerlander, K. K. K.; Köhler, L.; Huittinen, N. M.; Bok, F.; Steudtner, R.; Oschatz, C.; Vogel, M.; Stumpf, T.; Brunner, E.;

Originally published:

November 2020

Applied Geochemistry 126(2021), 104823

DOI: https://doi.org/10.1016/j.apgeochem.2020.104823

Sorption of Europium on Diatom Biosilica as Model of a "Green" Sorbent for *f*-Elements

Kaitlin Kim Karlotta Kammerlander‡[a], Lydia Köhler‡[a], Nina Huittinen [b], Robin Steudtner [b], Cathleen Oschatz [a1], Manja Vogel [b], Thorsten Stumpf [b], and Eike Brunner [a]*

[a] Chair of Bioanalytical Chemistry, Faculty of Chemistry and Food Chemistry, TU Dresden, Dresden 01062, Germany;

[b] Institute of Resource Ecology, Helmholtz-Zentrum Dresden-Rossendorf, Dresden 01328, Germany

1. Abstract

Removing *f*-elements from anthropogenically contaminated sites is a challenging, but ecologically important task. Some of these elements are not only radioactive, but also chemically toxic and can spread through various pathways in the environment. The present work investigates *f*-element sorption on biogenic silica, which may be a promising "green" material for remediation. Commercially available diatomaceous earth (DE) and the cleaned cell walls of the diatom species *Stephanopyxis turris* (*S.t.*) and *Thalassiosira pseudonana* (*T.p.*) are compared with artificial mesocellular foam (MCF) as porous silica reference material. Trivalent europium was chosen as model sorptive for chemically similar trivalent actinides. Accordingly, Eu(III) in concentrations of 10^{-3} M and 10^{-5} M was sorbed on the four silica materials at varying pH values. The zeta potentials of the implemented sorbents under the same conditions were determined. With time-resolved laser-induced fluorescence spectroscopy (TRLFS), two different uptake mechanisms can be discerned, surface adsorption and incorporation/precipitation.

KEYWORDS: biosilica; diatoms; europium; fluorescence; sorption

* Correspondence: eike.brunner@tu-dresden.de; Tel.: +49-351-463-3263.

‡ These authors contributed equally.

[1] currently: Max Planck Institute of Colloids and Interfaces, Potsdam 14476, Germany.

2. Introduction

The recovery of 4*f*-elements (lanthanides) and 5*f*-elements (actinides) from the environment is important from different perspectives. While these elements should be removed from anthropogenically contaminated sites, they also constitute valuable raw materials. These might be of increasing value as the natural resources become scarcer and more difficult to retrieve in the future.[1] Furthermore, studying the environmental interactions of lanthanides yields important information on the behavior of their radioactive analogs in the actinide series.

A possible approach for scavenging dissolved substances from the environment is to accumulate them via sorption. It is therefore indispensable to identify suitable sorbents, which should not only be efficient in accumulating the desired elements, but also offer ecological and economic advantages.[2,3] In this regard, biogenic materials often surpass artificial materials.[4]

The silica cell walls of diatoms exhibit several beneficial properties: They are hierarchically structured and porous, chemically and physically stable, and non-toxic.[5] Fossilized diatom cell walls (frustules) are frequently evaluated and applied as sorbents in the form of diatomite or diatomaceous earth (DE).[6] For example, this material has been considered for the pretreatment of radioactive wastewater.[7] Its specific surface area (SSA) is in the order of 30 to 40 $m^2\ g^{-1}$.[8] Apart from a high percentage of frustules of various diatom species, DE contains a considerable amount of other mineral compounds.[6]

In contrast, the cleaned cell wall material of axenically cultivated and harvested diatoms is much more homogeneous in terms of chemical composition as well as morphology (i.e. shape and size) of the particles. Furthermore, fresh diatom biosilica contains a higher amount of silanol groups (Si−OH). These are partly fused to siloxane groups (Si−O−Si) in aged biosilica like diatomite.[5] Consequently, fresh frustules constitute a more defined and thus preferable object for fundamental research like the luminescence spectroscopic studies in the current work. Fresh diatom biosilica is currently scarce, but it may become available as large-scale by-product of future food and oil production.[9] In contrast, diatomite is easily available as it can be extracted from abundant natural deposits.

In the present study, the sorption of trivalent lanthanide ions on both aged biosilica (diatomite) and fresh biosilica of two different diatom species was examined. To gain fresh biosilica, the two centric species *Stephanopyxis turris* (*S.t.*) and *Thalassiosira pseudonana* (*T.p.*) were axenically cultured in artificial seawater (ASW). *Stephanopyxis turris* is a wide-spread diatom species, inhabiting mainly temperate waters.[10] The cells are 20–100 µm long[10] and, therefore, suitable for diverse microscopical analysis methods. Their frustules exhibit a hierarchical structure of hexagonal pores, resulting in an SSA of ~60 $m^2\ g^{-1}$ for extracted biosilica.[8] *Thalassiosira pseudonana* grows fast in a wide temperate range and is resistant to environmental stress, resulting in an almost worldwide distribution of this diatom species.[11] The cylindrical cells are comparatively small with a diameter of 2–15 µm.[11] The cleaned frustules of this species exhibit an SSA of about 60–100 $m^2\ g^{-1}$, slightly higher than *S.t.*[8,12] The biogenic materials were compared with mesocellular foam (MCF), an abiogenic, synthetic silica.[13] Due to its mesoporous structure with pore diameters of 20–50 nm, it has a very high internal porosity with a SSA of 680 $m^2\ g^{-1}$.[14]

To evaluate these sorbents, europium was chosen as model sorptive. Eu(III) is often used as analog of trivalent actinide ions such as Cm(III) or Am(III).[15,16] Eu(III) also exhibits excellent luminescent properties, facilitating the structural analysis of its coordination compounds by fluorescence spectroscopy. The structure and surface charge of the sorbents as well as the Eu(III) loading and speciation were elucidated through scanning electron microscopy (SEM), zeta potential measurements, inductively coupled plasma optical emission spectroscopy (ICP-OES), and TRLFS.

3. Materials and Methods

3.1. Diatom Cultivation and Biosilica Extraction

DE (p.a.) was purchased from Merck and used as received.

Axenic diatom cultures were grown in 20 L batches of sterile-filtered artificial seawater (ASW) with a composition according to **Table A3** (appendix) at 20 °C. The cultivation vessels were illuminated with 1000 Lux in a 12 h/12 h light/dark cycle. To monitor cell growth, the Si concentration was analyzed colorimetrically via the molybdenum blue method.[17] After the Si concentration decreased below 5 µM, algae were harvested by centrifugation with a Hereaus Megafuge at 4000 rpm.

The resulting cell pellets were lysed to remove organic material from the silica frustule. For this purpose, 20 mL buffer solution (20 g L^{-1} sodium dodecyl sulfate (SDS), 37 g L^{-1} sodium ethylenediamine-tetraacetic acid (Na_2EDTA)) were added to the pellet, mixed and heated to 95 °C for 10 min. The suspension was centrifuged for 10 min at 4000 rpm in a Hereaus Biofuge primo and the supernatant was discarded afterwards. This lysis step was repeated until the supernatant appeared clear. Subsequently, the pellet was washed 5 times with Millipore water and then dried at -55 °C and 0.47 mbar in a Christ Alpha 1-4 LSCbasic freeze dryer.

In order to remove tightly bound or embedded organic residues from the lysed cells, the material was calcined in a muffle furnace for 5 h at 550 °C under air atmosphere.

3.2. Synthesis of MCF

MCF was synthesized according to the preparation method of Schmidt-Winkel et al. [13] Pluronic® P-123 (PEG-PPG-PEG block copolymer), ammonium fluoride, and 1,3,5-trimethylbenzene were heated to 35–40 °C in hydrochloric acid for at least 45 min. After adding tetraethoxysilane and retaining the temperature for another 20 h, the suspension was heated to 100 °C for 24 h. The solid material was filtered, dried, and calcined for 8 h at 500 °C.[13]

3.3. Zeta Potential Measurements

Zeta potentials of the silica sorbents were measured with a Zetasizer Nano Series device by Malvern Instruments. Therefore, about 5 mg of the solid was suspended in 2 mL 0.1 M $NaClO_4$. The pH values were adjusted to 2, 3, 4, 5, 6, 6.5, and 7 with NaOH and $HClO_4$.

3.4. Batch Sorption Experiments

For sorption experiments, Eu(III) solutions with a concentration of 10^{-3} M and 10^{-5} M were prepared from $EuCl_3 \cdot 6\,H_2O$ (99.99%, Sigma-Aldrich) and ultrapure water. 0.1 M $NaClO_4 \cdot H_2O$ (≥99.0% p.a., VWR) was chosen as background electrolyte. After adding 10 mL of the solutions to 10 mg of the respective sorbents, the suspensions were immediately adjusted to pH 3, 4, 5, 6, 6.5, and 7, respectively, with NaOH and $HClO_4$. After 3 days shaking at room temperature, the mixtures were centrifuged for 10 min at 4000 rpm in a Hereaus Biofuge primo.

3.5. SEM and EDX

After sorption, a small amount of the silica material was suspended in n-hexane and pipetted onto an aluminum pin stub. The dried samples were sputter-coated with gold and visualized in a Hitachi SU 8000 microscope (Hitachi). For energy-dispersive X-ray (EDX) spectroscopy, the peaks of the K series were used for Si and the peaks of the L series for Eu. The acceleration voltage was adjusted to 2–4 keV for imaging and 15–20 keV for EDX analysis/mapping. Exemplary results are shown in the appendix (**Figure A1**, **Figure A2**).

3.6. ICP-OES

The concentration of Eu in the supernatants after sorption was determined via ICP-OES. Therefore, samples with an initial Eu concentration c_0(Eu) of 10^{-3} M and 10^{-5} M were diluted in HNO_3 (5%) 1:1000 and 1:10, respectively. The resulting liquids were analyzed with an Optima 7000DV spectrometer (Perkin Elmer) utilizing the following parameters: high frequency power 1300 W, liquid flow 1.6 L min^{-1}, plasma gas flow 15 L min^{-1}, auxiliary gas flow 0.2 L min^{-1}, and nebulizer gas flow 0.65 L min^{-1}. The spectral line was 412.970 nm for radial detection of Eu.

3.7. TRLFS

All Eu species were indirectly and, thus, simultaneously excited at 394 nm to get an overview of their speciation in each sample as influenced by the conditions during sorption. TRLFS measurements were conducted at room temperature with a Nd:YAG pumped OPO laser system (Powerlite Precision II 9020 - PANTHER EX OPO, Continuum), a monochromator with a grating of 300 or 1200 lines mm^{-1} (Oriel MS 257) and a CCD camera (Andor iStar).

Fluorescence lifetimes were collected by monitoring the luminescence intensity as a function of delay time between laser pulse and acquisition. By integrating the individual spectra and plotting the results as a function of delay time, the fluorescence decay curves could be acquired. This data was analyzed with MATLAB (The MathWorks), OriginPro (OriginLab) and Andor Solis (Andor). To each lifetime value, the confidence interval of the fit (95% confidence level) is given.

In aqueous solution, the hydration shell effectively quenches Eu fluorescence lifetimes through an energy transfer to the OH vibrational overtones of the water molecules.[18] H_2O is progressively replaced when Eu ions coordinate with more sites to a sorbent material. Thus, the luminescence decay mechanism becomes less effective and luminescence lifetimes increase. The semi-empirical Horrocks equation[19] approximates the number of water molecules in the first coordination sphere as a function of the measured luminescence lifetime τ in ms as:

$$n(H_2O \pm 0.5) = 1.07\ \tau^{-1} - 0.62$$

Furthermore, luminescence decay curves (depicted in **Figure A4**, appendix) can be described using an exponential fit. The number of decay modes commonly corresponds to the number of luminescent species formed in a given sample. The integral band intensity ratio of the emission bands at about 620 nm and 590 nm, further denoted as $^7F_2/^7F_1$,[18] can be interpreted as an indicator of the strength of complexation. As the $^7F_2$ band is a hypersensitive transition, its increasing integral intensity changes the $^7F_2/^7F_1$ emission-band ratio of less than one (i.e., $^7F_1 > ^7F_2$) for the non-complexed aquo ion to more than one upon sorption (i.e., $^7F_1 < ^7F_2$).[18]

In addition to the $^7F_2/^7F_1$ ratio, some of the collected spectra show significant differences at varying pH values pointing towards the formation of more than one surface-sorbed Eu(III) species. Thus, the recorded spectra were deconvoluted as described in the literature to identify individual species.[16,20] Therefore, the spectrum of the Eu^{3+} aquo ion was subtracted from the original spectra. Alternatively, two spectra measured at consecutive pH values were compared with one another, i.e. the spectrum measured at a lower pH was subtracted from the spectrum at a higher pH. Some of the resulting difference spectra can be considered as single component spectra. These difference spectra were further subtracted from recorded spectra with additional species. Major species are further denoted as consecutively numbered species.

4. Results and Discussion

4.1. Zeta Potentials of the Sorbent Materials

Electrostatic interactions strongly affect the sorption of ions. Thus, not only the speciation of the sorptive, but also the charge of the sorbent is pivotal. The isoelectric point (pH(I)), i.e., the pH value at zero net electric charge, can be determined through zeta potential measurements.[21] In the current study, zeta potentials of the sorbent materials were measured at the same buffer concentrations and pH values as applied during the sorption experiments to assess possible changes in charge. The investigated pH range covers the mostly near-neutral pH of natural water bodies as well as acidic conditions characteristic for mine waters.[22] The zeta potentials of all sorbent materials (see **Figure 1**) above pH 4 are negative, facilitating the sorption of cations. Within the studied pH range of pH 3–7, a pH(I) can only be determined for MCF at pH 3–4. The zeta potential measurements of the diatom materials indicate an overall negative charge of the surface at any pH in the studied range. These findings agree with literature data reporting that the pH(I) of silica materials can vary from below 1 to 4 or may not exist.[23]

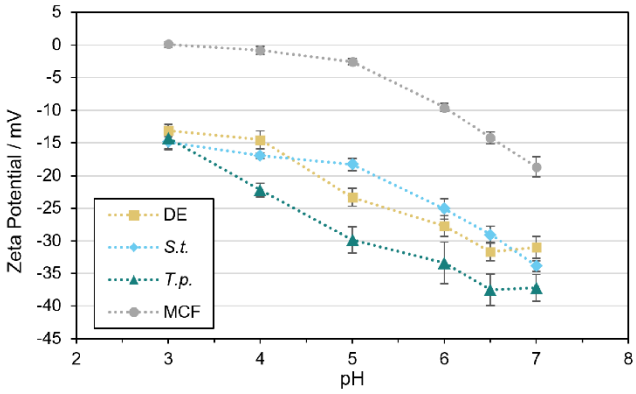

Figure 1. Zeta potential of different types of silica in 0.1 M $NaClO_4$ with varying pH value (error bars indicate the confidence interval at 95% confidence level, t-distribution).

For Eu(III), the Eu^{3+} aquo ion dominates the speciation in acidic media up to a pH of 6 (200 µM Eu)[24] or 7 (6.6 µM Eu)[25]. Small amounts of hydrolysis species, mainly $Eu(OH)^{2+}$, are also present at these pH values. At about pH 8, $Eu(CO_3)^+$ prevails in solutions in contact with air.[25] Negatively charged ions like $Eu(CO_3)_2^-$ and $Eu(CO_3)_3^{3-}$ become predominant only at higher pH values.[25] Thus, Eu sorption is favored in the pH range considered here. The zeta potential also provides information on the behavior of the particles in solution. Suspensions of small particles are considered as stable for zeta potentials with a modulus of 30 mV or higher. Between +30 mV and -30 mV, particles tend to agglomerate.[26] The

accessible surface area may then decrease. This threshold is at pH 6.0–6.5 for DE, at pH 6.5–7.0 for *S.t.* and at pH 5.0–6.0 for *T.p*.

4.2. Morphology of the Sorbent Materials

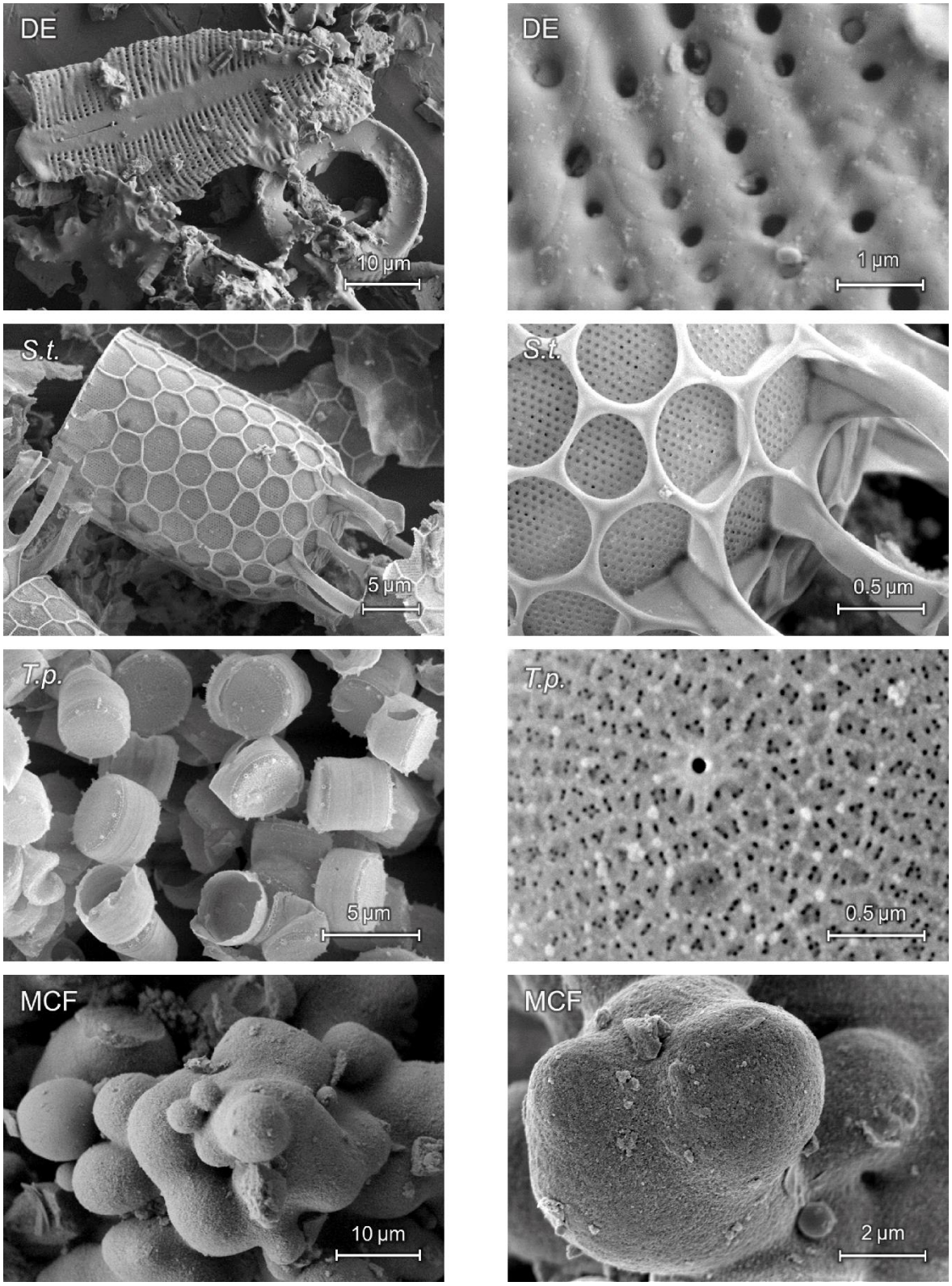

Figure 2. SEM images of the sorbent materials in different magnifications (2,500x up to 50,000x); acceleration voltage 2–4 kV.

The morphology of the utilized sorbent materials is very diverse, as can be seen from **Figure 2**. Diatomite consists of the cell walls originating from many different sedimented diatom species, which are fragmented to a large degree. The *S.t.* sample contains up to 100 µm long valves, i.e., comparably large particles. These cell walls exhibit three-dimensional, chamber-like pores with a larger opening on the outer side and a sieve plate with smaller pores on the inner side. In contrast, the smaller and flatter valves of *T.p.* with a diameter of about 5 µm contain a non-hierarchical pore system and are radially furrowed. Generally, the comparatively large pore diameters of the implemented sorbents DE,[8] *S.t.*,[27] *T.p.*[27] and MCF[27] should not restrict the sorption of the smaller Eu(III) ion. Only a negligible percentage below 3% of the pores is smaller than 2 nm, whereas over 50% of the pores are macropores.[27]

4.3. Batch Sorption – Quantitative Results

In general, the sorption of Eu(III) is influenced not only by the pH but also by the concentration of the sorptive. The sorption experiments were thus carried out at two different initial Eu(III) concentrations: 10^{-5} M and 10^{-3} M. Furthermore, the amount of sorbed Eu(III) on mixed silica materials can decrease at higher ionic strength through an increased number of ions that can screen the sorbent's surface or compete with sorptive ions.[28] This issue is taken into account in the current study by adding 0.1 M $NaClO_4$ as background electrolyte.

The surface site density and SSA determine the sorption capacity of sorbents. Considering the wide range of surface site density values reported in the literature for silica materials, a complete sorption of the Eu ions even at the higher initial concentration of 10^{-3} M is theoretically possible (see **Table A1**, appendix). The sorption efficiency is further influenced by the kind of available sites.

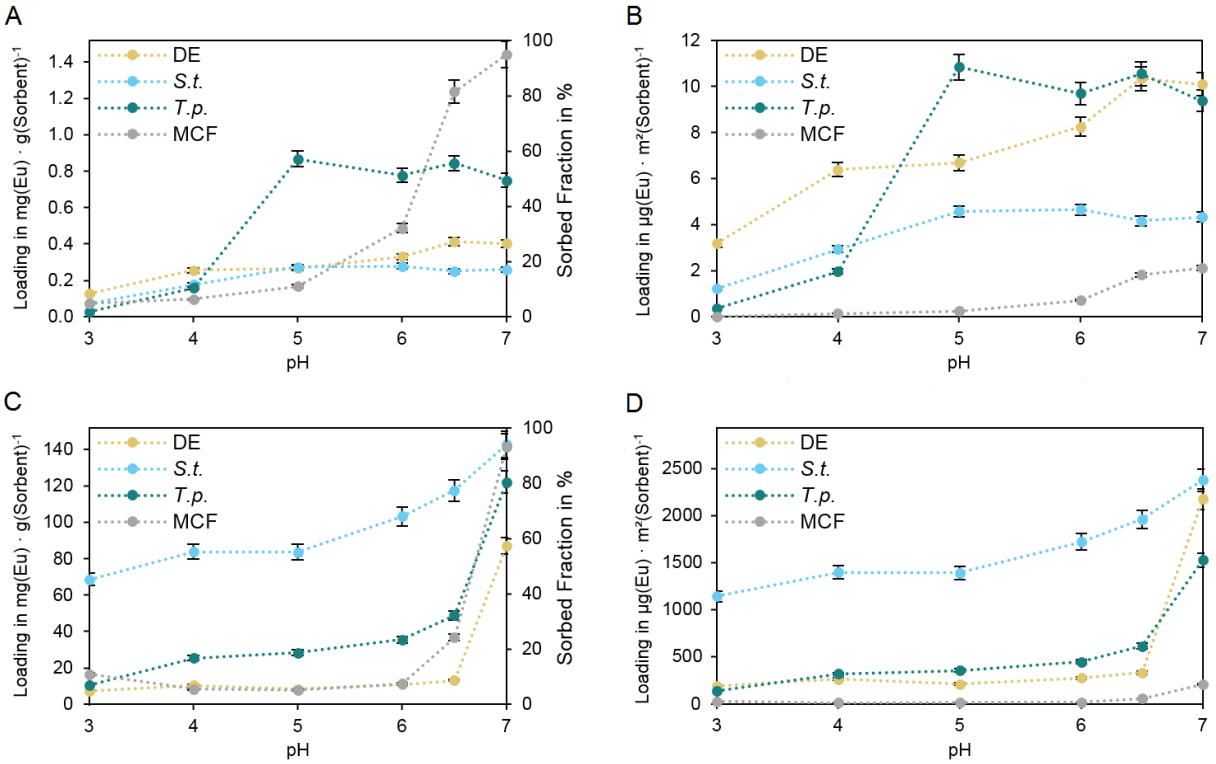

Figure 3. Quantitative analysis of the Eu sorption on different silica materials at varying pH value; **A,B**: $c_0(Eu) = 10^{-5}$ M; **C,D**: $c_0(Eu) = 10^{-3}$ M; **A,C**: sorbent loading normalized by mass; **B,D**: sorbent loading normalized to the SSA of the sorbents, whereby the following SSA values were used: DE

40 m² g^{-1}, *S.t.* 60 m² g^{-1}, *T.p.* 80 m² g^{-1}, MCF 680 m² g^{-1} (error bars indicate the confidence interval at 95% confidence level, t-distribution).

As shown in **Figure 3**, the sorbent loadings tend to increase with higher pH values at both initial Eu concentrations. One reason is the charge of the sorbent surfaces. According to the zeta potential measurements, the overall negative charges increase in the observed pH range at higher pH. In general, the loading scales with the initial Eu concentration. For biosilica, highest loadings are about 0.8 µg g^{-1} for 10^{-5} M (**Figure 3A,B)** and about 140 mg g^{-1} for 10^{-3} M Eu (**Figure 3C,D)**. Remarkably, though the artificial MCF exhibits a high SSA, its loading is not generally higher than that of the biogenic materials (except above pH 6 for c_0(Eu) = 10^{-5} M). *S.t.* shows high loadings over a large pH range for 10^{-3} M Eu. *T.p.* removes about half of the Eu at pH 5–6 and is thus the most effective sorbent under these conditions.

The determined sorbent loadings up to 140 mg g^{-1} are in the order of 1–100 mg g^{-1} that is usual for biosorbents.[29,30] As initial experiments with the used diatom species and general studies with living microalgae and dead algae biomass indicate,[4] the removal of Eu by diatoms may be increased if complete cells instead of cleaned cell walls were implemented. Containing amine, amide, carbonyl, and carboxyl among other functional groups, the organic compounds of the external cell surface exhibit a multitude of potential ligands.[4,31] Therefore, the sorption on whole diatom cells is a fascinating, but even more complex issue.

In **Figure 3B,D**, loadings are normalized to the SSA. This allows comparing the sorbent materials with respect to the quality of the sorbent surface rather than its size. Accordingly, the loading of the highly porous MCF is lower in this visualization (**Figure 3B,D**). At c_0(Eu) = 10^{-5} M, *T.p.* and DE are more efficient than *S.t.* biosilica. This situation changes at c_0(Eu) = 10^{-3} M, where *S.t.* accumulates the highest amount of Eu relative to the SSA. The comparatively large loadings of the diatom biosilica normalized to the SSA may also arise from a higher amount of silanol groups and other functionalities resulting from impurities. The presence of "foreign elements" such as Fe and Al – especially in DE –also influence the surface charge depending on mass ratio and pH.[32,33] Hence, the chemical advantages of the biosilica with respect to Eu sorption become evident.

Besides the sorption of Eu onto silanol groups and other functionalities, a precipitation of Eu can occur, for example in the form of Eu hydroxides. A similar mechanism is the partial dissolution of silica and reprecipitation or coprecipitation of Eu and Si containing compounds like Eu(III) silicate complexes.[34] Fresh diatom frustules like *S.t.* at c_0(Eu) = 10^{-3} M may act as a more effective seed for the formation of Eu salts. Especially the rapid uptake of Eu(III) visible in all sorption curves from pH 6.5 to 7.0 shows that the solubility limit is exceeded in this neutral region. This behavior has been reported in studies with a high Eu concentration before.[35] For this reason, the following TRLFS studies will focus on the lower initial Eu concentration of 10^{-5} M (for samples with c_0(Eu) = 10^{-3} M, see **Figure A3**, appendix).

4.4. TRLFS – Emission Spectra and Lifetimes

TRLFS was employed to gain further insight into the speciation of the Eu-silica sorbates. Eu(III) luminescence emission spectra collected at various pH values for the different silica materials are presented in **Figure 4**. Sorbent spectra show a considerably higher $^7F_2/^7F_1$ band intensity ratio compared with the spectra of the Eu^{3+} aquo ion (**Figure 4**). This implies a change in the coordination environment of the sorbed cation and subsequent attachment at the surface by inner-sphere sorption.

The spectra of the *T. p.* sorbate closely resemble each other over the entire investigated pH range (**Figure 4C**). However, these composite spectra reveal some minor changes in the shoulder, visible in the $^7F_2$ band at approximately 620 nm, indicating the presence of two Eu(III) species at the *T.p.* silica surface. In the deconvolution process, a single component spectrum of "species 1" could be extracted from the spectra measured at pH 3 and 4 (**Figure 5A**).

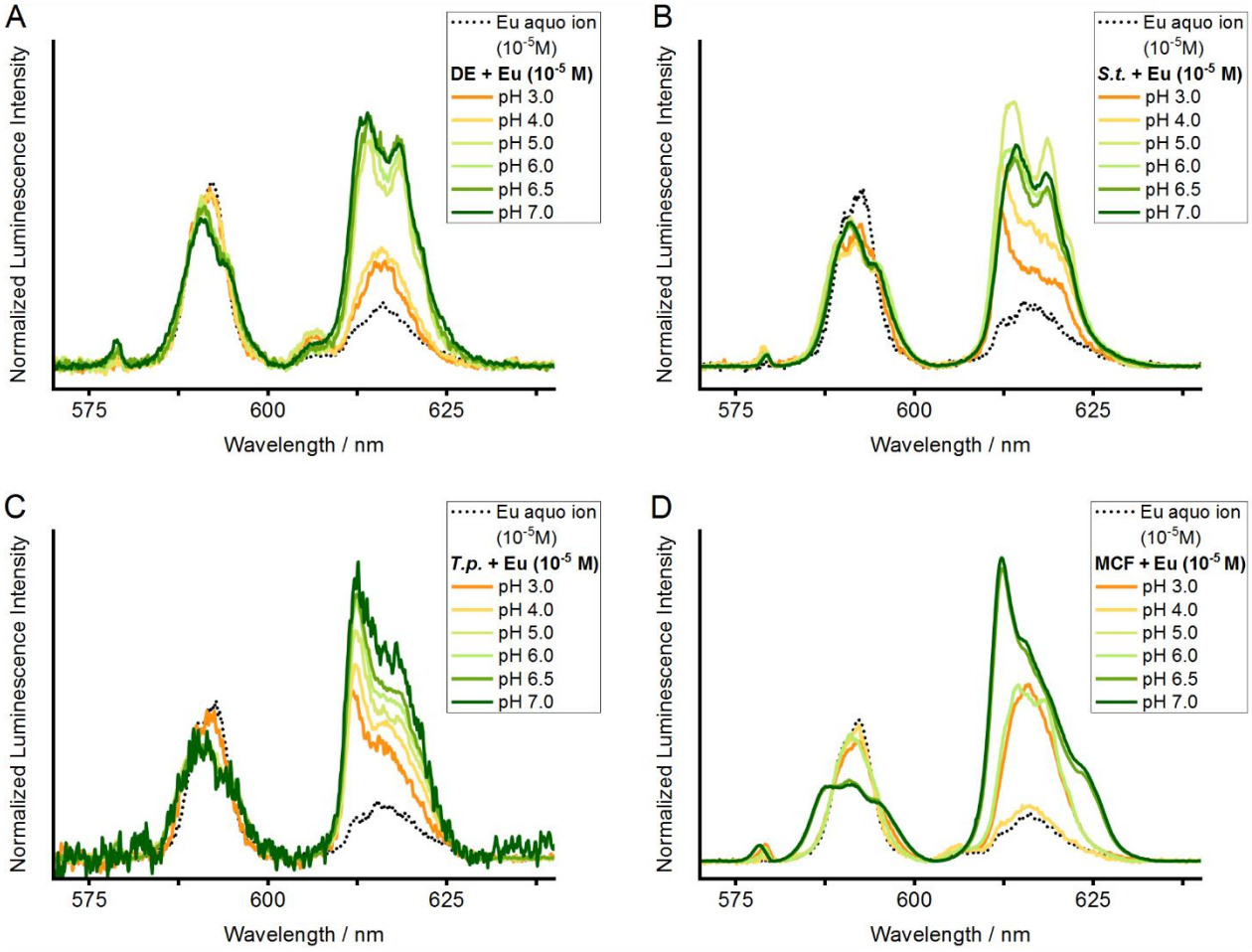

Figure 4. Luminescence emission spectra of the solid biosilica samples after sorption of c_0(Eu) = 10^{-5} M at different pH values; spectra normalized to $^7F_1$ integrated band intensity. A: DE, B: *S.t.*, C: *T.p.*, D: MCF.

Above pH 4, the spectra cannot be explained solely with this single component spectrum, indicating the presence of a second Eu(III) species further denoted as "species 2" (**Figure 5A**). The Eu(III) luminescence for the *T.p.* silica solid phase decays biexponentially with a short-lived and a long-lived component with lifetimes of about 230 µs ± 20 µs (species 1) and 740 µs ± 50 µs (species 2), respectively. This corroborates the presence of two species in the system. Though additional quenching mechanisms might be introduced by transition metals such as iron due to the sorbent materials' natural origin,[36] the Horrocks equation is tentatively applied to calculate the number of water molecules in the first coordination sphere. For species 1, 4.0 ± 0.5 H_2O entities could be calculated, indicating the loss of half of the hydration sphere. Thus, this short-lived species is consistent with an inner-sphere complex found for Eu(III) sorption on inorganic sorbents like kaolinite.[37] In accordance, the emission spectrum of this component is similar to Eu(III) spectra sorbed on non-biogenic silica reported in the literature.[34,35]

In contrast, species 2 is surrounded by approximately 0.8 ± 0.5 H_2O in the first coordination sphere. Incorporation processes typically lead to a full loss of the primary hydration sphere as found for Cm(III) incorporation in siliceous bulk[38] or Eu(III) incorporation in hectorite[34]. However, partial hydration of one to two water molecules has been described e.g. for Eu(III) incorporation at grain boundaries of bioapatite[39] or in calcite[40]. Other reasons for a small number of H_2O in the first coordination sphere are surface precipitation of Eu(III) species or additional coordination of the Eu(III) surface complex to silicates. The latter phenomenon has been reported for Cm(III) complexes on the surfaces of kaolinite[20] and illite[41]. Based on the collected luminescence data for Eu(III) attachment on *T.p.*, a final conclusion about the attachment mode at the interface cannot be drawn.

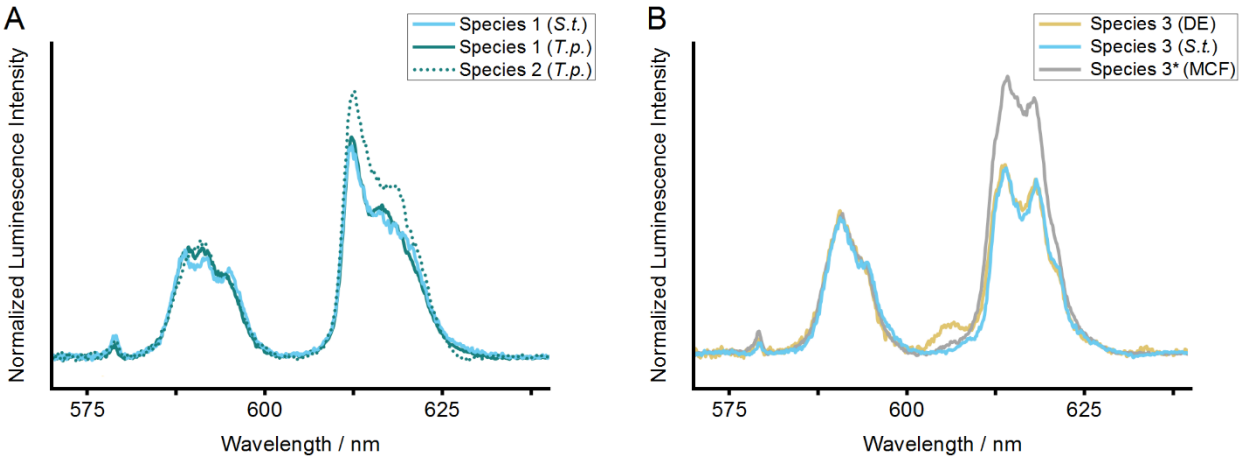

Figure 5. Extracted luminescence emission spectra; spectra normalized to $^7F_1$ integrated band intensity. A: examples for species 1 in *S.t.* and *T.p.* (solid line) and example for species 2 in *T.p.* (dotted line), B: examples for species 3 in DE and *S.t.* and species 3* in MCF.

For the second diatom species *S.t.* (**Figure 4B**) below pH 5, spectra similar to those extracted for *T.p.* (species 1 and 2) can be obtained after deconvolution (**Figure 5A**). The corresponding lifetimes of 230 µs ± 20 µs and 740 µs ± 50 µs indicate that a surface-sorbed Eu(III) complex and an incorporated/precipitated species are both present, as found in *T.p*. Hence, the fresh, biogenic silica materials exhibit the same two Eu species, but their ratios differ. At near neutral pH, only a small amount of species 1 and 2 can be detected in the *S.t.* material compared to a more acidic suspension.

In addition, *S.t.* exhibits an additional species further denoted as "species 3" (**Figure 5B**). At pH 5 and higher, this species is dominating the spectra of the *S.t.* sorbates. Upon the formation of this species, the luminescence lifetimes change to a long-lived component of 940 µs ± 30 µs and a short-lived component of 58 µs ± 4 µs. The extraordinarily short lifetime of the second component – below that of the non-complexed Eu^{3+} aquo ion (about 110 µs)[18] – must be caused by a luminescence quenching effect. As mentioned above, quenching may occur in the presence of certain transition metal impurities such as iron,[36] but also between Eu centers when the local Eu concentration is high enough, e.g. in a precipitate. In the relevant aqueous system with SiO_2 and Eu, a precipitate can be composed of Eu hydroxides, Eu silicates or mixed/ternary forms thereof. For example, Eu hydroxides exhibit an extremely short lifetime due to quenching of the hydroxyl groups in addition to the short-range Eu-Eu self-quenching effects.[42] Especially Eu self-quenching has previously been shown to result in biexponential lifetimes despite the presence of only one Eu(III) environment.[43] Using the Horrocks equation, the lifetime of 940 µs would yield 0.5 ± 0.5 H_2O molecules in the first coordination sphere. As the longer component of a precipitated species is likely to be influenced by self-quenching, the actual lifetime can be expected to be even higher. This implies a full loss of the Eu^{3+} hydration sphere.

Generally, these (co-)precipitated and incorporated/intercalated species can result from a partial dissolution of the silica surface. While silica dissolves faster in bases, the dissolution rate is similar within an acidic medium from pH 3–6, as previously shown for quartz and silica glass.[44,45] Foreign ions can influence the dissolution process depending on their ionic radius[46] or the frequency of solvent exchange around the aqueous cations.[47] For example, aluminum – which is a typical component of DE – can reduce the dissolution of silica.[48] In contrast, Eu(III) can promote the dissolution of silica, as is known for alkaline and earth alkaline metal ions.[35] Dissolved Si can form Eu(III) silicate complexes like $[Eu(OSi(OH)_3]^{2+}$ and $[Eu(OSi(OH)_3)_2]^{+}$.[49] Thus, an increased dissolution of impure silica materials at high Eu concentrations may result in a higher amount of intercalated Eu, e.g., through co-precipitation and redeposition of Si and Eu on the sorbent surface.

For the third biogenic silica material, DE (**Figure 4A**), emission spectra resemble mainly those collected for *S.t.* at pH 5 and above. Hence, species 3 dominates the emission spectra of DE samples. In contrast to *S.t.* and *T.p.*, the surface-sorbed species 1 is not apparent in the emission spectra of DE. Though, the time-resolved data indicate the presence of a minor species with a lifetime of 270 µs ± 30 µs, corresponding to silanol surface sorption. The reduced amount of this species is probably caused by a lower concentration of silanol groups in diatomite.[5] Generally, the SSA of DE is comparatively low. Thus, the number of sites on the DE surface is also lower if the site density of the biogenic silicates is similar. In addition to the medium lifetime, an especially short and long lifetime with 27 µs ± 3 µs and 1020 µs ± 70 µs can be found. As previously explained, these lifetimes can result from the same incorporated/precipitated species due to self-quenching.

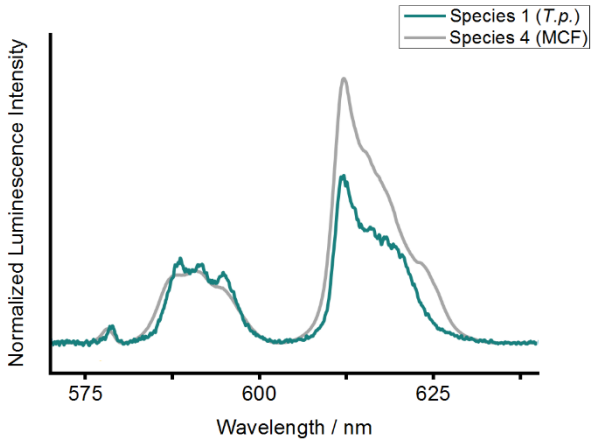

Figure 6. Extracted luminescence emission spectra; spectra normalized to $^7F_1$ integrated band intensity: examples for species 1 in *T.p.* and species 4 in MCF.

Finally, the luminescence spectra of the three aforementioned biogenic silica materials can be compared with the luminescence data obtained for the synthetic silica, MCF (**Figure 4D**). Below pH 5, the spectra of the mesoporous MCF show species equivalent to species 3 with respect to the band shape and particularly the splitting of the $^7F_2$ band (see **Figure 5B**). Though, the $^7F_2/^7F_1$ ratio is higher in the spectra of MCF, indicating a stronger complexation. Accordingly, this species of MCF is referred to as "species 3*". The corresponding triexponential decay correlates with lifetimes of 46 µs ± 16 µs, 180 µs ± 60 µs and 1150 µs ± 170 µs.

In addition, other species can be identified at pH 5 and above: the luminescence decays biexponentially with lifetimes of 150 µs ± 10 µs and 780 µs ± 60 µs, which is further denoted as "species 4". Its threefold splitting of the $^7F_1$ band resembles the even more pronounced splitting of species 1 as depicted in **Figure 6**. Again, the $^7F_2/^7F_1$ ratio is higher in the spectra of MCF. In addition, the $^7F_0$ band is slightly more pronounced in the spectra of MCF and DE, suggesting a lower degree of symmetry of the

formed Eu species. The $^7F_2$ band intensity in the MCF spectra may be increased through a higher Eu loading as MCF exhibits a relatively high SSA and, thus, a higher total amount of silanol groups, i.e. binding sites. The large surface could also lead to a higher partial dissolution of the MCF material and subsequent co-precipitation with Eu.

Consequently, multiple differing Eu species are discernable in the silica sorbates (summarized in **Table A2**, appendix). The extremely short-lived components with lifetimes below 60 µs in species 3 (DE, *S.t.*) and 3* (MCF) result from self-quenching. The components with lifetimes between 150 µs and 270 µs in species 1 (*T.p.*, *S.t.*), 3 (DE), 3* (MCF) and 4 (MCF) are probably Eu species sorbed on silanol groups. These surface-sorbed species are predominantly found in the *T.p.* samples, coinciding with the highest SSA of the biogenic materials. When the SSA decreases as it is the case for *S.t.* silica, species 1 decreases in abundance until it vanishes for DE with the smallest SSA. Instead, the amount of partially incorporated or precipitated Eu(III) species increases. About one water molecule remains in the inner-sphere of the species with a lifetime of about 740 µs to 780 µs as found in species 2 (*T.p.*, *S.t.*) and 4 (MCF). In contrast, the hydration sphere is absent in the species with a lifetime between 940 µs and 1150 µs in species 3 (DE, *S.t.*) and 3* (MCF). The long lifetimes are in the range of those reported for Eu incorporated into minerals, suggesting an amorphous Eu-silica phase.[34]

5. Conclusions

In this study, Eu(III) was sorbed onto diatom biosilica and a synthetic silica material. Due to their negative surface charge, the sorption of cations is facilitated. Resulting sorbent loadings are up to 140 mg g^{-1}. With TRLFS, the formed Eu(III) species could be characterized: reversible surface sorption is predominant for *S.t.* (acid conditions) and *T.p.*, while irreversible incorporation or precipitation occurs for *S.t.* (near neutral pH), DE and MCF. Loadings could be increased by modifying the pore system or using whole cells in future studies. Altogether, diatom biosilica is a promising "green" material for scavenging *f*-elements in aqueous solution.

6. Abbreviations

ASW, artificial seawater; DE, diatomaceous earth; EDX, energy-dispersive X-ray spectroscopy; ICP-OES, inductively coupled plasma optical emission spectroscopy; MCF, mesocellular foam; p.a., *pro analysi*; PEG, polyethylene glycol; PPG, polypropylene glycol; SEM, scanning electron microscopy; SSA, specific surface area; *S.t.*, *Stephanopyxis turris*; *T.p.*, *Thalassiosira pseudonana*; TRLFS, time-resolved laser-induced fluorescence spectroscopy.

7. Acknowledgement

This research was performed in cooperation between TU Dresden and the Institute of Resource Ecology of the Helmholtz-Zentrum Dresden-Rossendorf. The synthesis of MCF by Martin Oschatz, at that time working at the Chair of Inorganic Chemistry I, TU Dresden, is gratefully acknowledged. The authors also thank Andrea Brünner (Chair of Inorganic Chemistry II, TU Dresden) and Susanne Goldberg (Chair of Physical Chemistry, TU Dresden) for SEM/EDX measurements as well as Christiane Leudolph (Chair of Bioanalytical Chemistry, TU Dresden) for the elemental analyses with ICP-OES. Further thanks are due to Prof. N. Kröger (B CUBE, TU Dresden) for providing equipment for Zeta potential measurements.

8. Funding Sources

This work was supported by the BMBF Germany (Federal Ministry of Education and Research) within the research activity project FENABIUM (02NUK046A). The BMBF had no involvement in study design; in the collection, analysis and interpretation of data; in the writing of the report; and in the decision to submit the article for publication.

9. Declaration of Interest

The authors declare that they have no known competing financial interests or personal relationships that could have appeared to influence the work reported in this paper.

10. CRediT Authorship Contribution Statement

Kaitlin Kim Karlotta Kammerlander: Formal analysis, Investigation, Writing - Original Draft, Visualization; **Lydia Köhler:** Formal analysis, Investigation, Writing - Original Draft, Visualization; **Nina Huittinen:** Formal analysis, Writing - Review & Editing; **Robin Steudtner:** Writing - Review & Editing; **Cathleen Oschatz:** Writing - Review & Editing; **Manja Vogel:** Writing - Review & Editing; **Thorsten Stumpf:** Resources, Writing - Review & Editing, Supervision; **Eike Brunner:** Resources, Writing - Review & Editing, Supervision; **All authors:** Conceptualization.

11. References

(1) de Boer, M. A.; Lammertsma, K. Scarcity of Rare Earth Elements. *ChemSusChem* **2013**, *6* (11), 2045–2055. https://doi.org/10.1002/cssc.201200794.

(2) He, J.; Chen, J. P. A Comprehensive Review on Biosorption of Heavy Metals by Algal Biomass: Materials, Performances, Chemistry, and Modeling Simulation Tools. *Bioresour. Technol.* **2014**, *160*, 67–78. https://doi.org/10.1016/j.biortech.2014.01.068.

(3) Götzke, L.; Schaper, G.; März, J.; Kaden, P.; Huittinen, N.; Stumpf, T.; Kammerlander, K. K. K.; Brunner, E.; Hahn, P.; Mehnert, A.; et al. Coordination Chemistry of F-Block Metal Ions with Ligands Bearing Bio-Relevant Functional Groups. *Coord. Chem. Rev.* **2019**, *386*. https://doi.org/10.1016/j.ccr.2019.01.006.

(4) Leong, Y. K.; Chang, J. S. Bioremediation of Heavy Metals Using Microalgae: Recent Advances and Mechanisms. *Bioresour. Technol.* **2020**, *303*, 122886–122929. https://doi.org/10.1016/j.biortech.2020.122886.

(5) Smol, J. P.; Stoermer, E. F. *The Diatoms: Applications for the Environmental and Earth Sciences*, 2nd ed.; Cambridge University Press: Cambridge, 2010.

(6) *Industrial Minerals & Rocks: Commodities, Markets, and Uses*, 7th ed.; Kogel, J. E., Trivedi, N. C., Barker, J. M., Krukowski, S. T., Eds.; Society for Mining, Metallurgy, and Exploration, 2006.

(7) Yongfeng, Jiang; Linshuang, Wang; Jian, Pu ; Yuntang, L. Filtering Medium for Removing Micro Radioactive Substances in Water and Preparation Method Thereof. CN101628222 (B), 2011.

(8) Fischer, C. Materialwissenschaftliches Potential Biologischer Silikate: Zucht Verschiedener Mikroalgen - Charakterisierung Und Anwendung von Biosilikaten. 2017.

(9) Tang, D. Y. Y.; Khoo, K. S.; Chew, K. W.; Tao, Y.; Ho, S. H.; Show, P. L. Potential Utilization of Bioproducts from Microalgae for the Quality Enhancement of Natural Products. *Bioresour.*

Technol. **2020**, *304*, 122997. https://doi.org/10.1016/j.biortech.2020.122997.

(10) Kraberg, A.; Baumann, M.; Dürselen, C.-D. *Coastal Phytoplankton: Photo Guide for Northern European Seas*; Verlag Dr. Friedrich Pfeil: München, 2010.

(11) Kipp, R. M.; McCarthy, M.; Fusaro, A. Thalassiosira pseudonana (Hustedt) Hasle and Heimdal, (1957) 1970 https://nas.er.usgs.gov/queries/GreatLakes/FactSheet.aspx?SpeciesID=1692, Revision Date: 9/12/2019, (accessed Oct 1, 2020).

(12) Köhler, L.; Machill, S.; Werner, A.; Selzer, C.; Kaskel, S.; Brunner, E. Are Diatoms "green" Aluminosilicate Synthesis Microreactors for Future Catalyst Production? *Molecules* **2017**, *22* (12). https://doi.org/10.3390/molecules22122232.

(13) Schmidt-Winkel, P.; Wayne W. Lukens, J.; Zhao, D.; Yang, P.; Chmelka, B. F.; Stucky, G. D. Mesocellular Siliceous Foams with Uniformly Sized Cells and Windows. *J. Am. Chem. Soc.* **1999**, *121* (1), 254–255. https://doi.org/10.1021/JA983218I.

(14) Fischer, C.; Adam, M.; Mueller, A. C.; Sperling, E.; Wustmann, M.; van Pée, K.-H.; Kaskel, S.; Brunner, E. Gold Nanoparticle-Decorated Diatom Biosilica: A Favorable Catalyst for the Oxidation of D-Glucose. *ACS Omega* **2016**, *1* (6), 1253–1261.

(15) Stumpf, T.; Curtius, H.; Walther, C.; Dardenne, K.; Ufer, K.; Fanghänel, T. Incorporation of Eu(III) into Hydrotalcite: A TRLFS and EXAFS Study. *Environ. Sci. Technol.* **2007**. https://doi.org/10.1021/es0624873.

(16) Jordan, N.; Demnitz, M.; Lösch, H.; Starke, S.; Brendler, V.; Huittinen, N. Complexation of Trivalent Lanthanides (Eu) and Actinides (Cm) with Aqueous Phosphates at Elevated Temperatures. *Inorg. Chem.* **2018**, *57* (12), 7015–7024. https://doi.org/10.1021/acs.inorgchem.8b00647.

(17) Iler, R. K. *The Chemistry of Silica. Solubility, Polymerization, Colloid and Surface Properties, and Biochemistry.*; John Wiley and Sons, 1979.

(18) Binnemans, K. Interpretation of Europium(III) Spectra. *Coord. Chem. Rev.* **2015**, *1–45*, 295.

(19) Horrocks, W. D.; Sudnick, D. R. Lanthanide Ion Probes of Structure in Biology. Laser-Induced Luminescence Decay Constants Provide a Direct Measure of the Number of Metal-Coordinated Water Molecules. *J. Am. Chem. Soc.* **1979**, *101* (2), 334–340. https://doi.org/10.1021/ja00496a010.

(20) Huittinen, N.; Rabung, T.; Schnurr, A.; Hakanen, M.; Lehto, J.; Geckeis, H. New Insight into Cm(III) Interaction with Kaolinite - Influence of Mineral Dissolution. *Geochim. Cosmochim. Acta* **2012**, *99*, 100–109. https://doi.org/10.1016/j.gca.2012.09.032.

(21) Preocanin, T.; Kallay, N. *Point of Zero Charge and Surface Charge Density of TiO2 in Aqueous Electrolyte Solution as Obtained by Potentiometric Mass Titration*; 2006; Vol. 79.

(22) Ayora, C.; Macías, F.; Torres, E.; Lozano, A.; Carrero, S.; Nieto, J.-M.; Pérez-López, R.; Fernández-Martínez, A.; Castillo-Michel, H. Recovery of Rare Earth Elements and Yttrium from Passive-Remediation Systems of Acid Mine Drainage. *Environ. Sci. Technol.* **2016**, *50* (15), 8255–8262. https://doi.org/10.1021/acs.est.6b02084.

(23) Kosmulski, M. The PH Dependent Surface Charging and Points of Zero Charge. VII. Update. *Adv. Colloid Interface Sci.* **2018**, *251*, 115–138. https://doi.org/10.1016/J.CIS.2017.10.005.

(24) Runde, W.; Meinrath, G.; Kim, J. I. A Study of Solid-Liquid Phase Equilibria of Trivalent Lanthanide and Actinide Ions in Carbonate Systems. *Radiochim. Acta* **1992**, *58–59* (1), 93–100. https://doi.org/10.1524/ract.1992.5859.1.93.

(25) Plancque, G.; Moulin, V.; Toulhoat, P.; Moulin, C. Europium Speciation by Time-Resolved Laser-Induced Fluorescence. *Anal. Chim. Acta* **2003**, *478* (1), 11–22. https://doi.org/10.1016/S0003-2670(02)01486-1.

(26) Lowry, G. V.; Hill, R. J.; Harper, S.; Rawle, A. F.; Hendren, C. O.; Klaessig, F.; Nobbmann, U.; Sayre, P.; Rumble, J. Guidance to Improve the Scientific Value of Zeta-Potential Measurements in NanoEHS. *Environ. Sci. Nano* **2016**, *3* (5), 953–965. https://doi.org/10.1039/C6EN00136J.

(27) Begum, G.; Oschatz, C.; Oschatz, M.; Kaskel, S.; Brunner, E.; Kröger, N. Influence of Silica Architecture on the Catalytic Activity of Immobilized Glucose Oxidase. *Bioinspired, Biomim. Nanobiomaterials* **2019**, *8* (1), 72–80. https://doi.org/10.1680/jbibn.18.00002.

(28) Polubesova, T.; Nir, S. Modeling of Organic and Inorganic Cation Sorption by Illite. *Clays Clay Miner.* **1999**, *47* (3), 366–374. https://doi.org/10.1346/CCMN.1999.0470313.

(29) Abdolali, A.; Guo, W. S.; Ngo, H. H.; Chen, S. S.; Nguyen, N. C.; Tung, K. L. Typical Lignocellulosic Wastes and By-Products for Biosorption Process in Water and Wastewater Treatment: A Critical Review. *Bioresour. Technol.* **2014**, *160*, 57−66. https://doi.org/10.1016/j.biortech.2013.12.037.

(30) Wan Ngah, W. S.; Hanafiah, M. A. K. M. Removal of Heavy Metal Ions from Wastewater by Chemically Modified Plant Wastes as Adsorbents: A Review. *Bioresour. Technol.* **2008**, *99* (10), 3935−3948. https://doi.org/10.1016/j.biortech.2007.06.011.

(31) Bilal, M.; Rasheed, T.; Sosa-Hernández, J. E.; Raza, A.; Nabeel, F.; Iqbal, H. M. N. Biosorption: An Interplay between Marine Algae and Potentially Toxic Elements—A Review. *Mar. Drugs* **2018**, *16* (2). https://doi.org/10.3390/md16020065.

(32) Waseem, M.; Mustafa, S.; Naeem, A.; Koper, G. J. M.; Salah-ud-Din. Physiochemical Properties of Mixed Oxides of Iron and Silicon. *J. Non. Cryst. Solids* **2010**, *356* (50–51), 2704–2708. https://doi.org/10.1016/J.JNONCRYSOL.2010.09.055.

(33) La Parola, V.; Deganello, G.; Scirè, S.; Venezia, A. M. Effect of the Al/Si Atomic Ratio on Surface and Structural Properties of Sol-Gel Prepared Aluminosilicates. *J. Solid State Chem.* **2003**, *174* (2), 482–488. https://doi.org/10.1016/S0022-4596(03)00321-9.

(34) Pieper, H.; Bosbach, D.; Panak, P. J.; Rabung, T.; Fanghänel, T. Eu (III) Coprecipitation with the Trioctahedral Clay Mineral, Hectorite. *Clays Clay Miner.* **2006**, *54* (1), 45–53. https://doi.org/10.1346/CCMN.2006.0540106.

(35) Takahashi, Y.; Murata, M.; Kimura, T. Interaction of Eu(III) Ion and Non-Porous Silica: Irreversible Sorption of Eu(III) on Silica and Hydrolysis of Silica Promoted by Eu(III). *J. Alloys Compd.* **2006**, *408–412*, 1246–1251. https://doi.org/10.1016/J.JALLCOM.2005.04.120.

(36) Tan, X.; Fang, M.; Wang, X. Sorption Speciation of Lanthanides/Actinides on Minerals by TRLFS, EXAFS and DFT Studies: A Review. *Molecules* **2010**, *15* (11), 8431–8468. https://doi.org/10.3390/molecules15118431.

(37) Huittinen, N.; Rabung, T.; Andrieux, P.; Lehto, J.; Geckeis, H. A Comparative Batch Sorption and Time-Resolved Laser Fluorescence Spectroscopy Study on the Sorption of Eu(III) and Cm(III) on Synthetic and Natural Kaolinite. *Radiochim. Acta* **2010**, *98* (9–11), 613–620. https://doi.org/10.1524/ract.2010.1761.

(38) Stumpf, S.; Stumpf, T.; Lützenkirchen, J.; Walther, C.; Fanghänel, T. Immobilization of Trivalent Actinides by Sorption onto Quartz and Incorporation into Siliceous Bulk: Investigations by TRLFS. *J. Colloid Interface Sci.* **2008**, *318* (1), 5–14. https://doi.org/10.1016/j.jcis.2007.09.080.

(39) Holliday, K.; Handley-Sidhu, S.; Dardenne, K.; Renshaw, J.; Macaskie, L.; Walther, C.; Stumpf, T.

A New Incorporation Mechanism for Trivalent Actinides into Bioapatite: A TRLFS and EXAFS Study. *Langmuir* **2012**, *28* (8), 3845–3851. https://doi.org/10.1021/la300014a.

(40) Hellebrandt, S. E.; Hofmann, S.; Jordan, N.; Barkleit, A.; Schmidt, M. Incorporation of Eu(III) into Calcite under Recrystallization Conditions. *Sci. Rep.* **2016**, *6* (33137). https://doi.org/10.1038/srep33137.

(41) Schnurr, A.; Marsac, R.; Rabung, T.; Lützenkirchen, J.; Geckeis, H. Sorption of Cm(III) and Eu(III) onto Clay Minerals under Saline Conditions: Batch Adsorption, Laser-Fluorescence Spectroscopy and Modeling. *Geochim. Cosmochim. Acta* **2015**, *151*, 192–202. https://doi.org/10.1016/J.GCA.2014.11.011.

(42) Runde, W.; Van Pelt, C.; Allen, P. G. Spectroscopic Characterization of Trivalent F-Element (Eu, Am) Solid Carbonates. *J. Alloys Compd.* **2000**, *303–304*, 182–190. https://doi.org/10.1016/S0925-8388(00)00665-4.

(43) Huittinen, N.; Arinicheva, Y.; Schmidt, M.; Neumeier, S.; Stumpf, T. Using Eu^{3+} as an Atomic Probe to Investigate the Local Environment in $LaPO_4$–$GdPO_4$ Monazite End-Members. *J. Colloid Interface Sci.* **2016**, *483*, 139–145. https://doi.org/10.1016/J.JCIS.2016.08.027.

(44) Crundwell, F. K. On the Mechanism of the Dissolution of Quartz and Silica in Aqueous Solutions. *ACS Omega* **2017**, *2* (3), 1116–1127. https://doi.org/10.1021/acsomega.7b00019.

(45) Brady, P. V.; Walther, J. V. Kinetics of Quartz Dissolution at Low Temperatures. *Chem. Geol.* **1990**, *82*, 253–264. https://doi.org/10.1016/0009-2541(90)90084-K.

(46) Plettinck, S.; Chou, L.; Wollast, R. Kinetics and Mechanisms of Dissolution of Silica at Room Temperature and Pressure. *Mineral. Mag.* **1994**, *58A* (2), 728–729. https://doi.org/10.1180/minmag.1994.58a.2.116.

(47) Dove, P. M.; Nix, C. J. The Influence of the Alkaline Earth Cations, Magnesium, Calcium, and Barium on the Dissolution Kinetics of Quartz. *Geochim. Cosmochim. Acta* **1997**, *61* (16), 3329–3340. https://doi.org/10.1016/S0016-7037(97)00217-2.

(48) Dixit, S.; Cappellen, P. Van; Bennekomb, A. J. Processes Controlling Solubility of Biogenic Silica and Pore Water Build-up of Silicic Acid in Marine Sediments. *Mar. Chem.* **2001**, *73* (3–4), 333–352.

(49) Kar, A. S.; Tomar, B. S.; Godbole, S. V.; Manchanda, V. K. Time Resolved Fluorescence Spectroscopy and Modeling of Eu(III) Sorption by Silica in Presence and Absence of Alpha Hydroxy Isobutyric Acid. *Colloids Surfaces A Physicochem. Eng. Asp.* **2011**, *378* (1–3), 44–49. https://doi.org/10.1016/J.COLSURFA.2011.01.039.